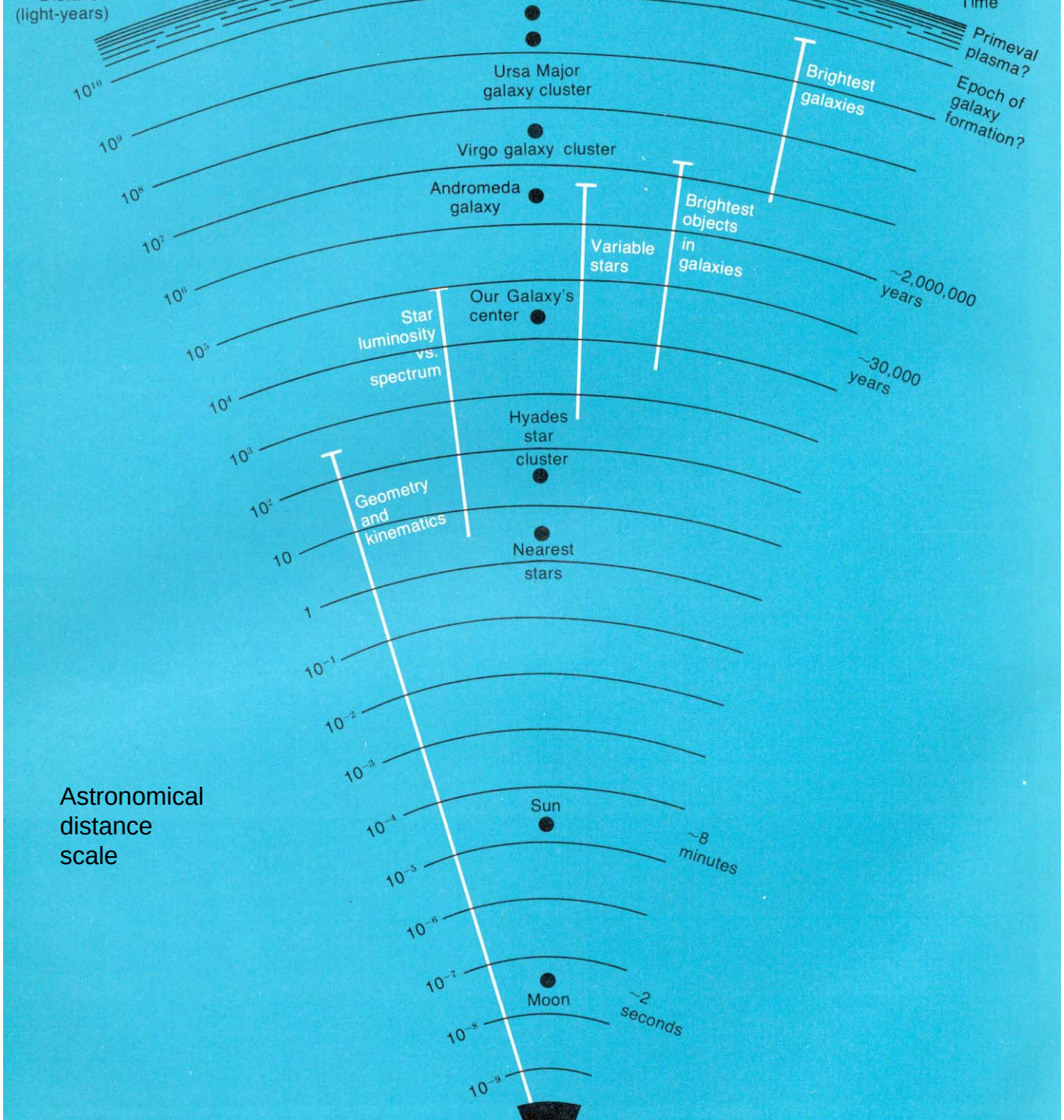

Astronomical distance scale

Lund composite Milky Way

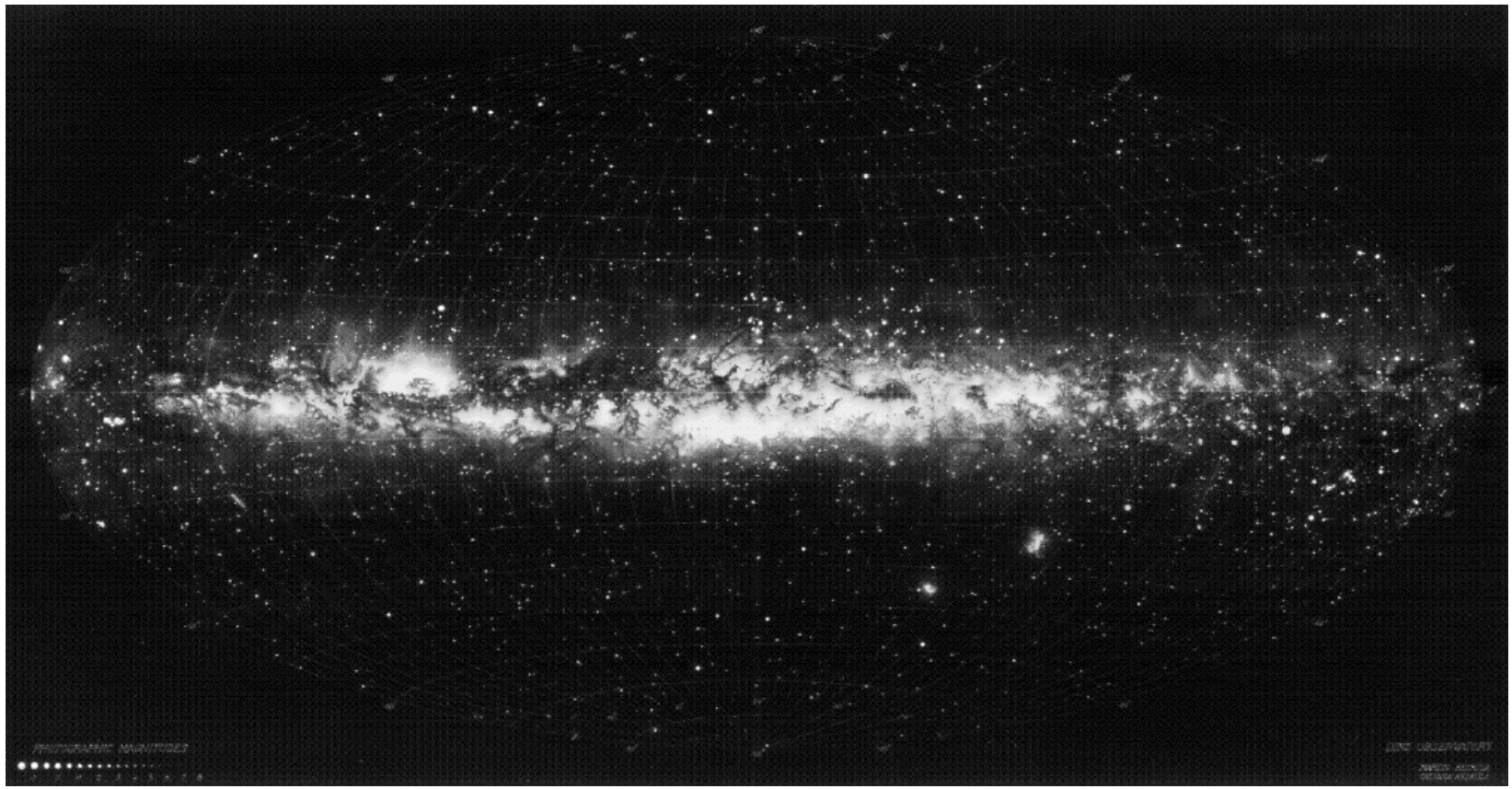

Black Hole in the galactic center

A. Ghez

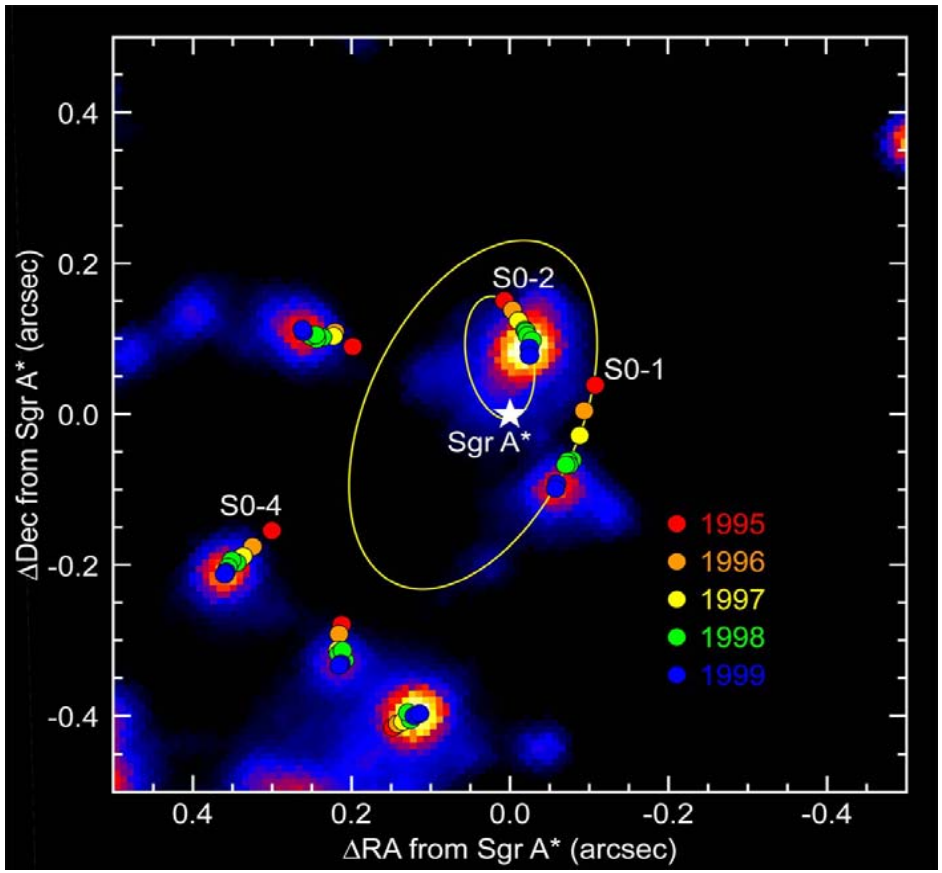

Andromeda Galaxy

Spiral Galaxies

M100 Galactic Nucleus

Hubble Space Telescope
Wide Field Planetary Camera 2

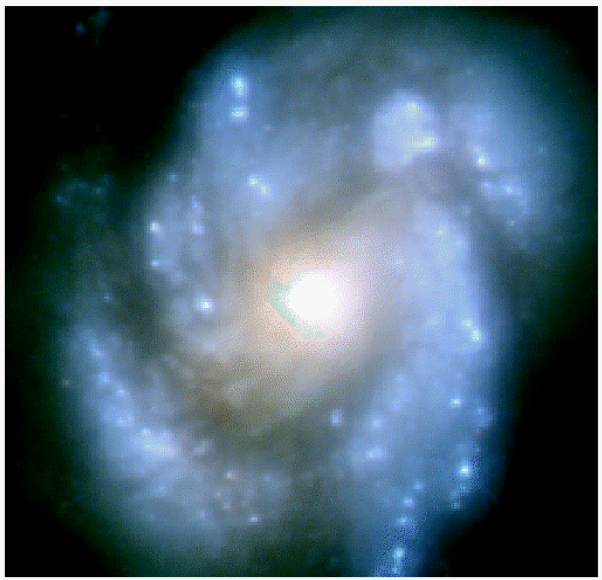

Wide Field Planetary Camera 1

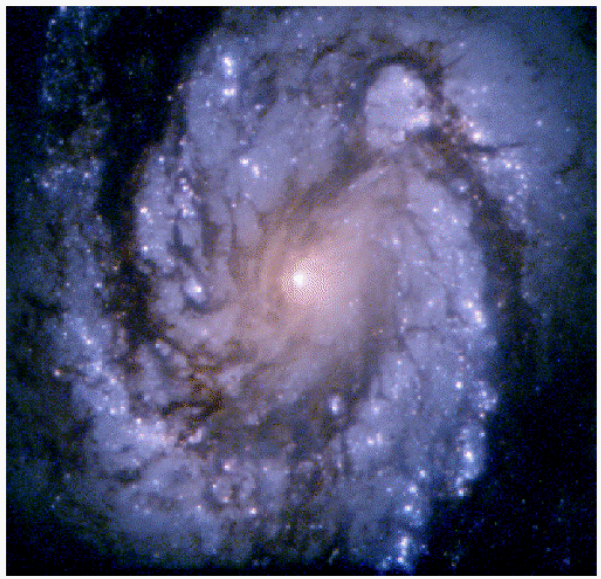

Wide Field Planetary Camera 2

Barred spiral galaxy

Coma cluster of galaxies

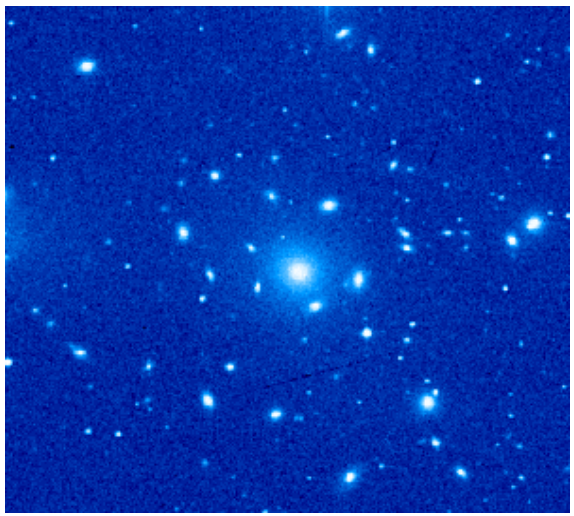

Coma Cluster of Galaxies

VIRGO cluster of galaxies

Red shift vs luminosity

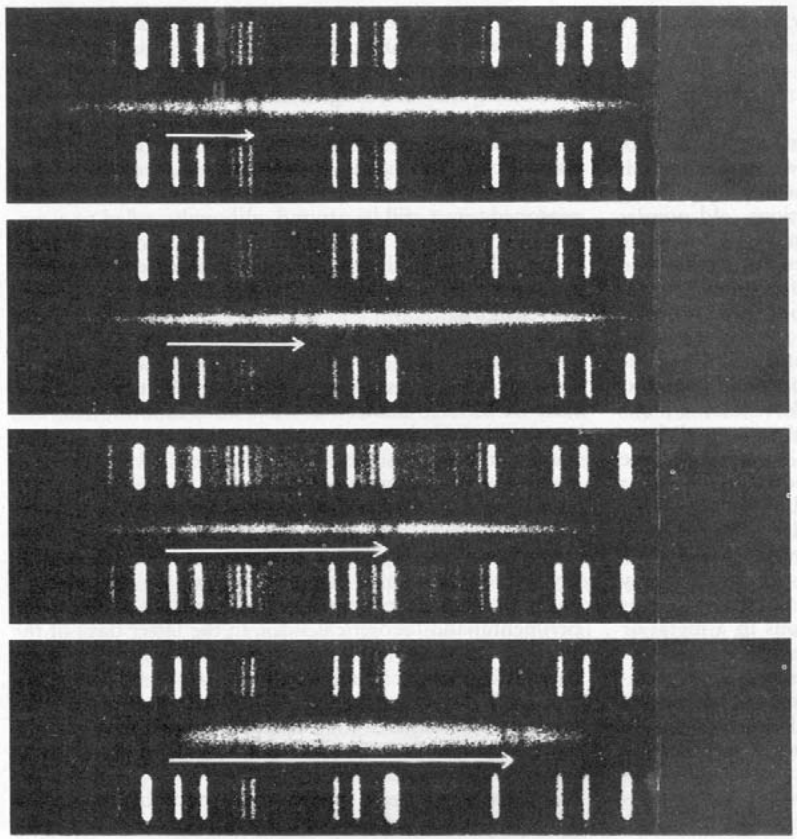

The relation between redshift and distance for four galaxies. In each spectrum, an arrow shows the shift in two calcium lines. If this shift is due to a recession velocity relative to the earth, then a galaxy in Ursa Major (uppermost spectrum in the illustration) is rushing away from us at 15,000 kilometers per second. The recession velocity is currently taken to be 50 km/sec for every million parsecs (3.25 million light-years) of the distance from earth to the galaxy. Accordingly, 15,000 km/sec corresponds to a distance of 10^9 light-years. The second spectrum is that of a galaxy in Corona Borealis; its redshift corresponds to a velocity of 22,000 km/sec and a distance of 1.4×10^9 light-years. The third spectrum is that of a galaxy in Bootes (39,000 km/sec; 2.5×10^9 light-years). The fourth is that of a galaxy in Hydra (61,000 km/sec; 3.96×10^9 light-years).

Hubble line

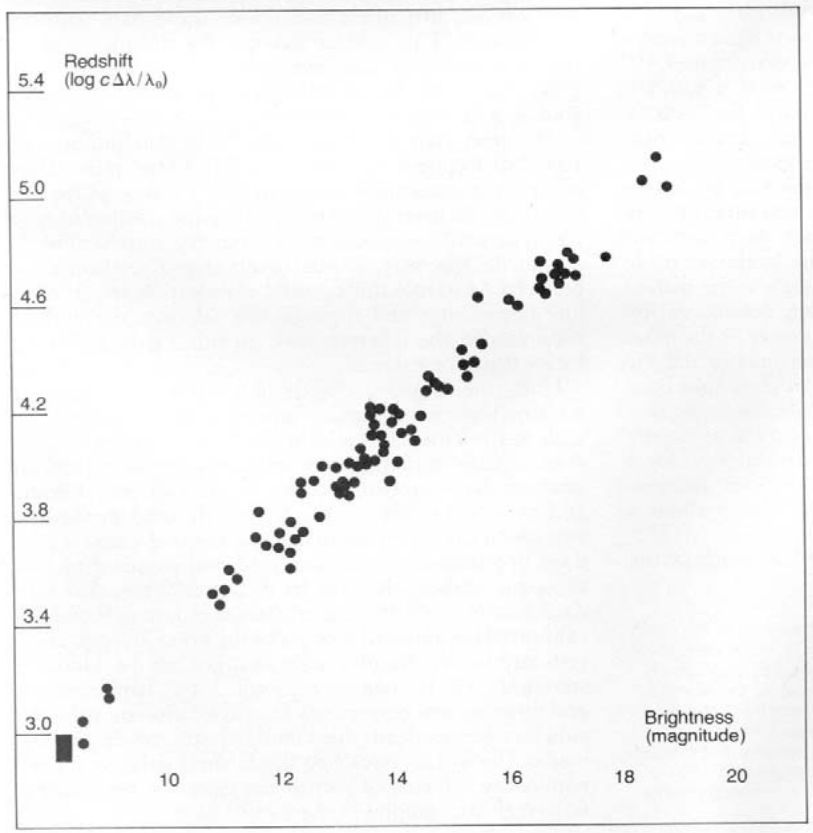

A Hubble diagram, using Sandage's data, that shows the wavelength shift vs. corrected magnitude for the brightest galaxy in each of 84 galaxy clusters. Increasing magnitude corresponds to fainter and more distant sources. The original Hubble data would lie within the small box near the origin.

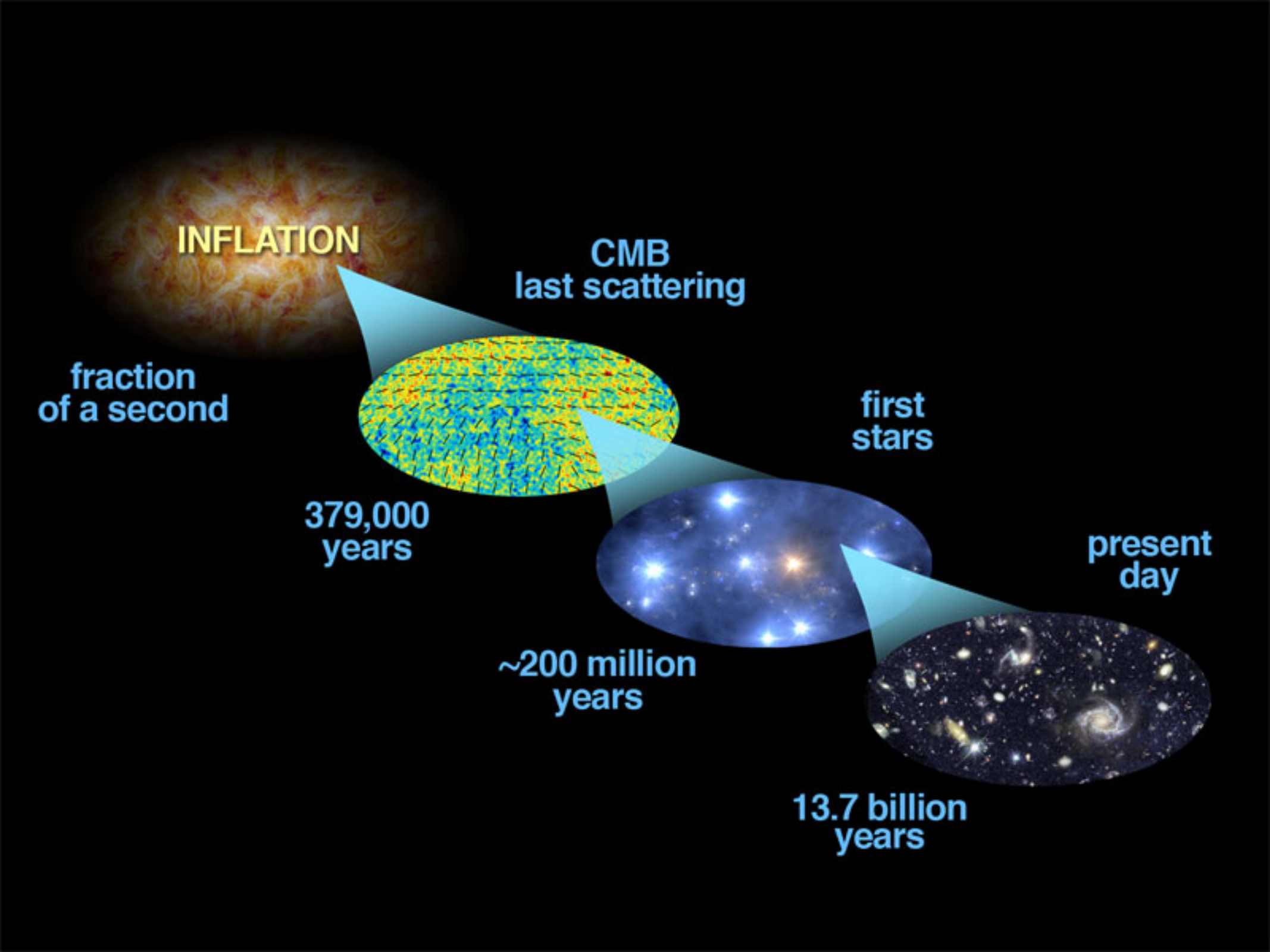
INFLATION
CMB
last scattering
fraction
of a second
379,000
years
first
stars
~200 million
years
present
day
13.7 billion
years

COBE Temperature Maps

Dipole

Dipole removed

Dipole and galaxy removed

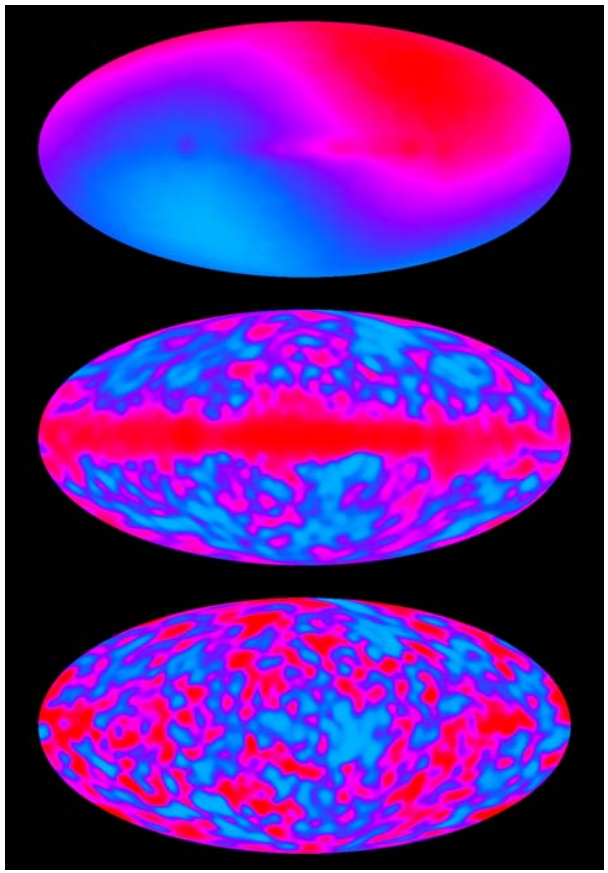

WMAP Composite map

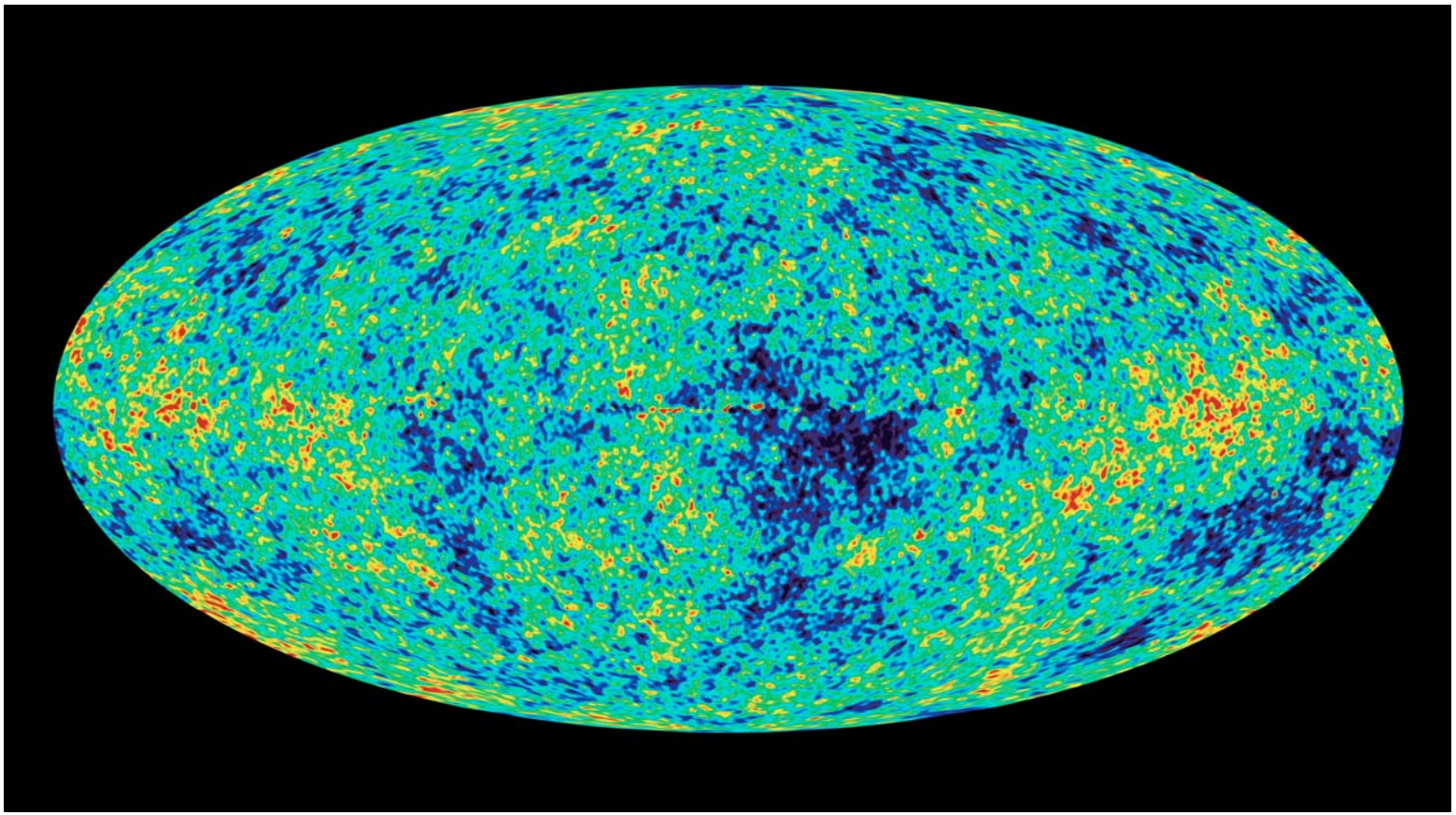

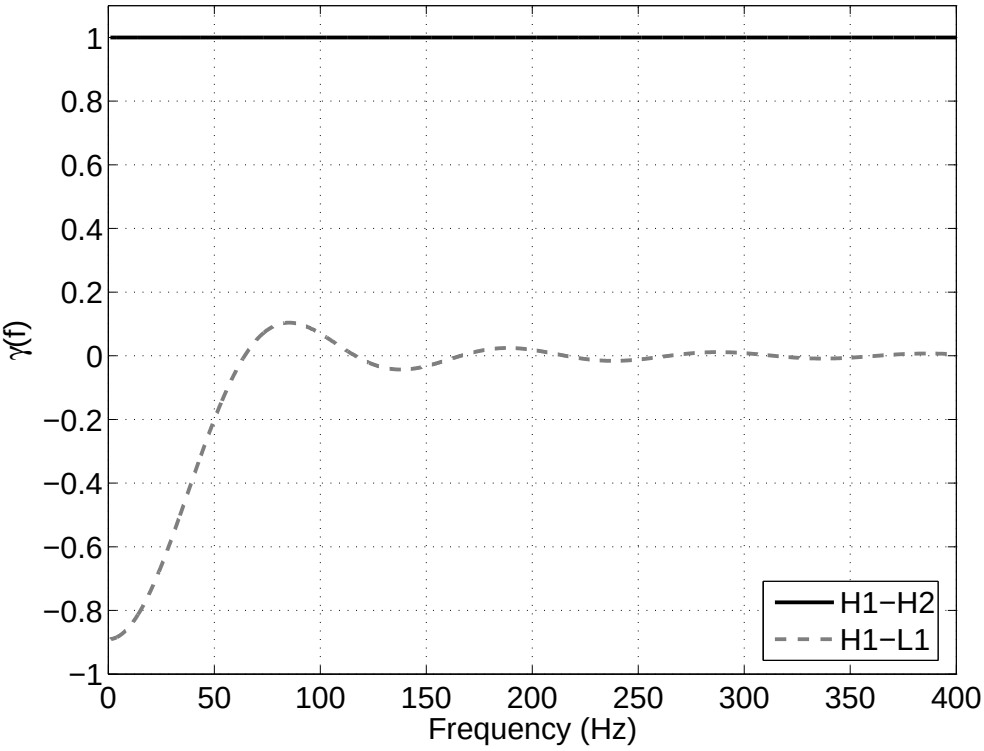

Fig. 2.— Overlap reduction function for the Hanford-Hanford pair (black solid) and for the Hanford-Livingston pair (gray dashed).

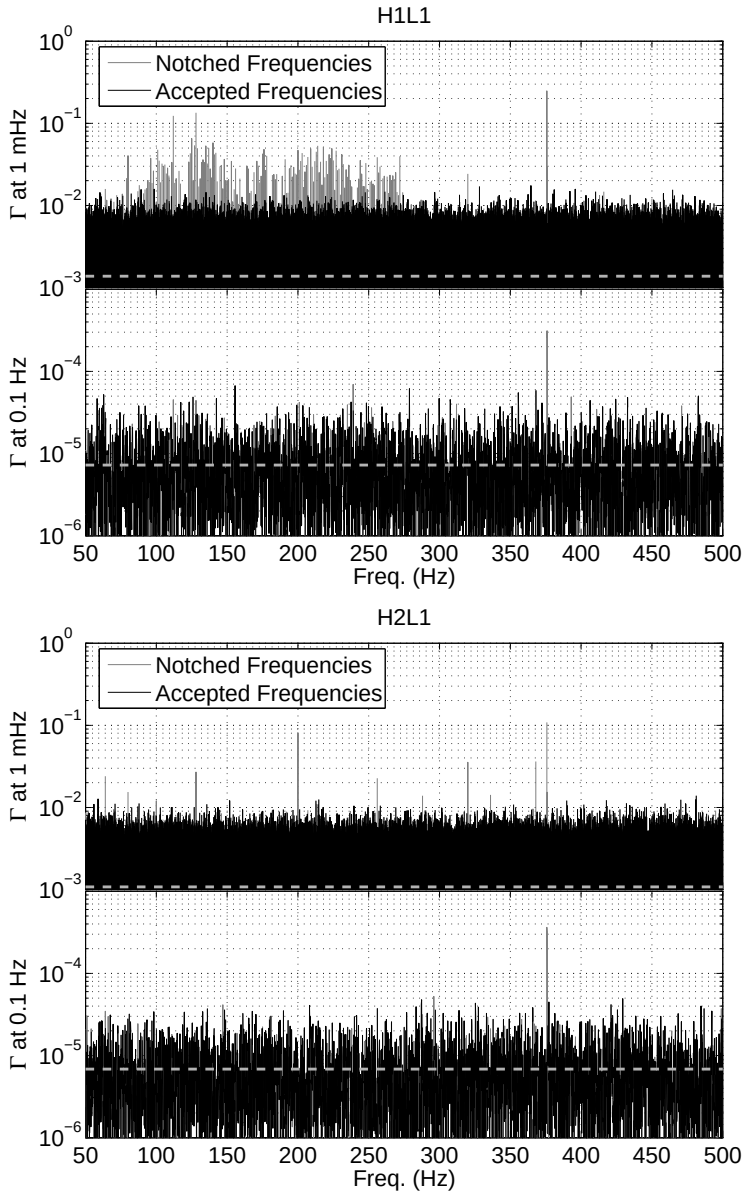

Fig. 3.— Coherence calculated for the H1L1 pair (top) and for the H2L1 pair (bottom) over all of S4 data for 1 mHz resolution and 100 mHz resolution. The horizontal dashed lines indicate $1/N_{avg}$ - the expected level of coherence after averaging over N_{avg} time-periods with uncorrelated spectra. The line at 376 Hz is one of the simulated pulsar lines.

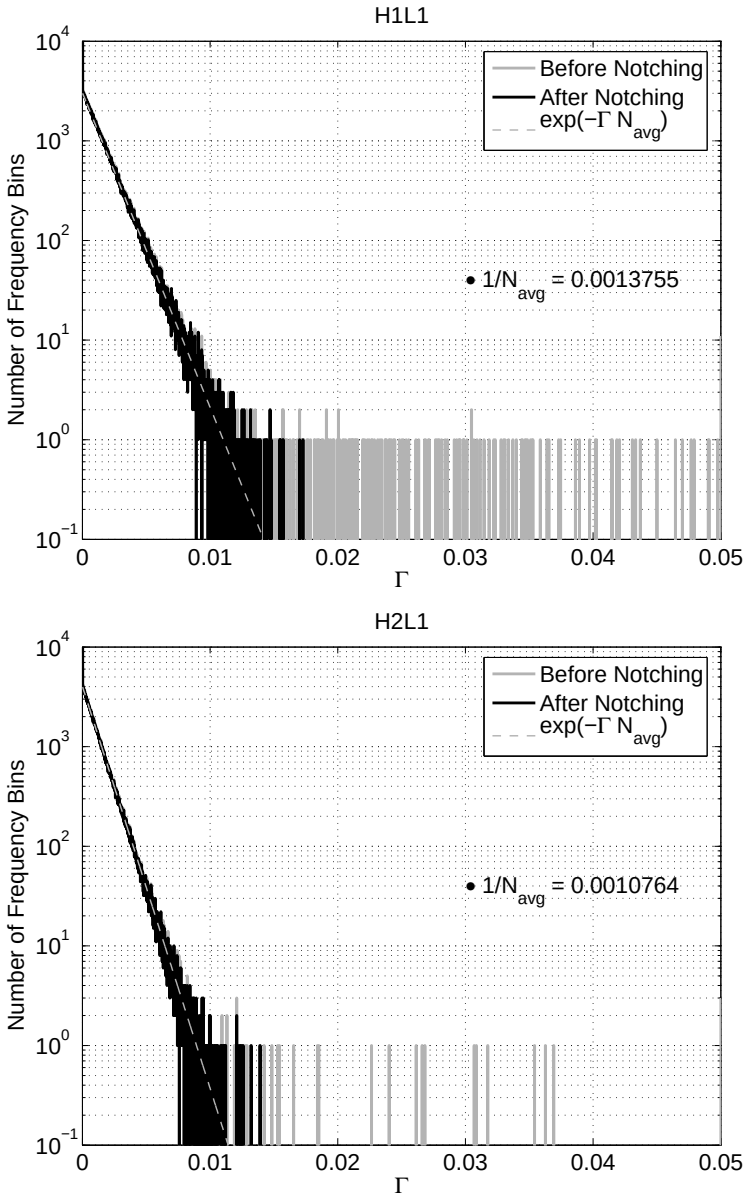

Fig. 4.— Histogram of the coherence for H1L1 (top) and H2L1 (bottom) at 1 mHz resolution follows the expected exponential distribution, with exponent coefficient $1/N_{avg}$, where N_{avg} is the number of time-periods over which the average is made.

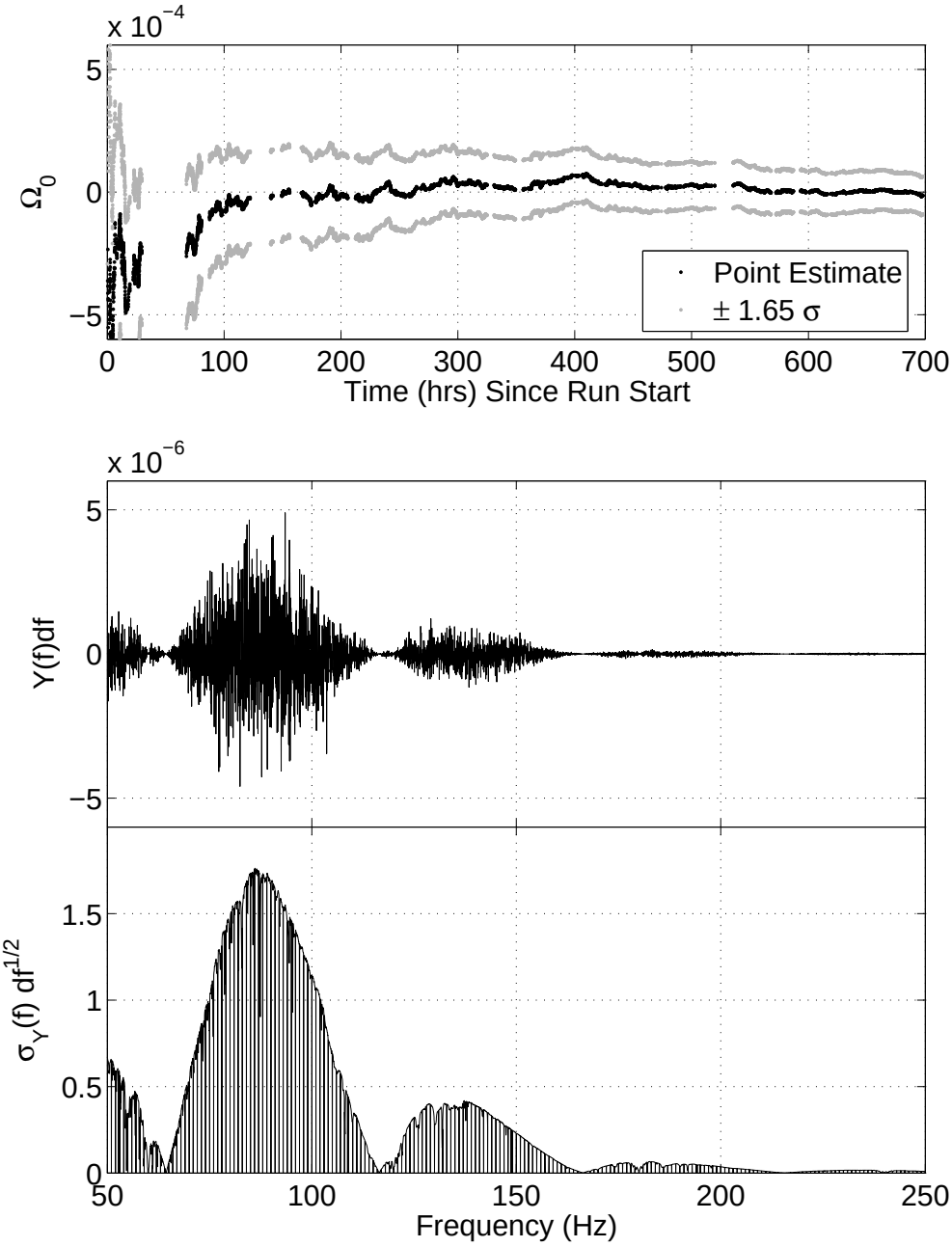

Fig. 8.— H1L1, 192-sec analysis with $\zeta = 0.3$. Top: Cummulative estimate of Ω_0 is shown as a function of time. Middle: cross-correlation spectrum $Y(f)$. Bottom: theoretical uncertainty $\sigma_Y(f)$ as a function of frequency.

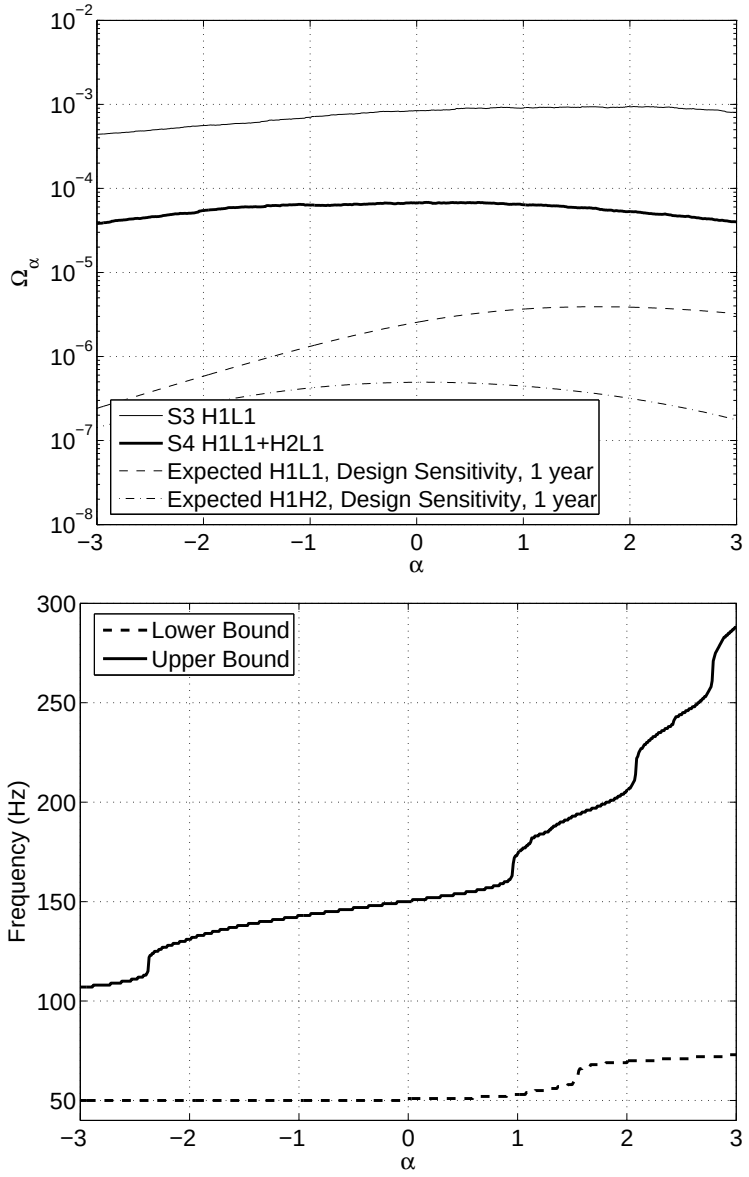

Fig. 11.— Top: 90% UL on Ω_α as a function of α for S3 H1L1 and S4 H1L1+H2L1 combined, and expected final sensitivities of LIGO H1L1 and H1H2 pairs, assuming LIGO design sensitivity and one year of exposure. Bottom: Frequency band as a function of α for the S4 result.

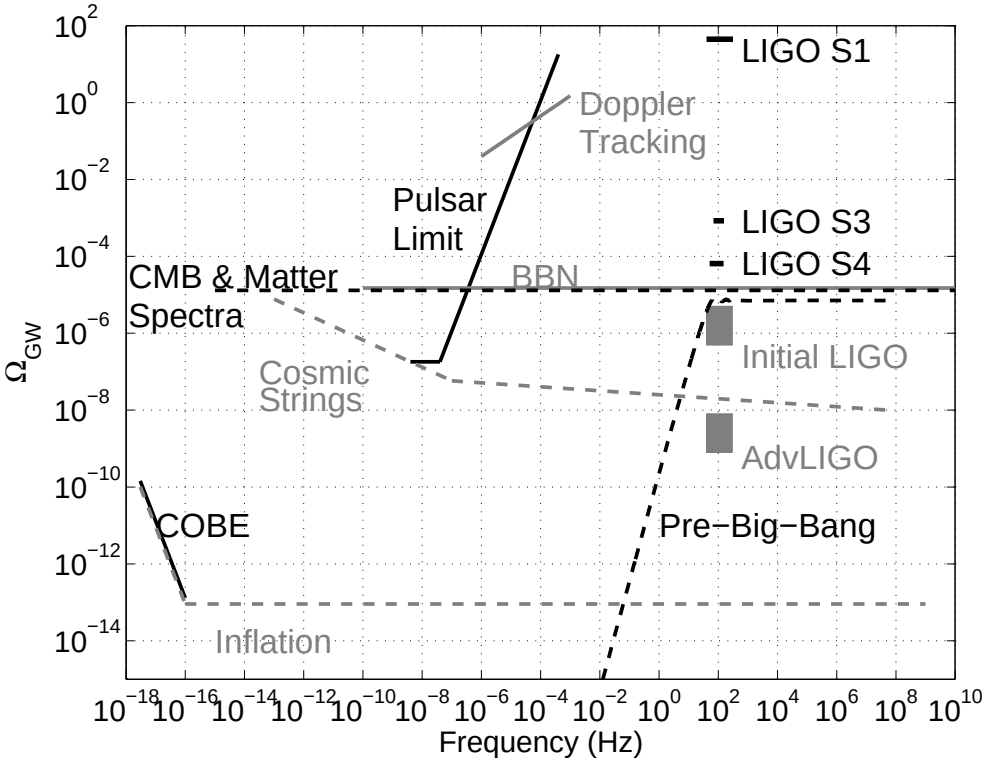

Fig. 14.— Landscape plot (see text for details). The curves corresponding to inflationary, cosmic-string, and pre-big-bang models are examples; significant variations of the predicted spectra are possible as the model parameters are varied. The bounds labeled "BBN" and "CMB and Matter Spectra" apply to the integral of the GW spectrum over the frequency range spanned by the corresponding lines.

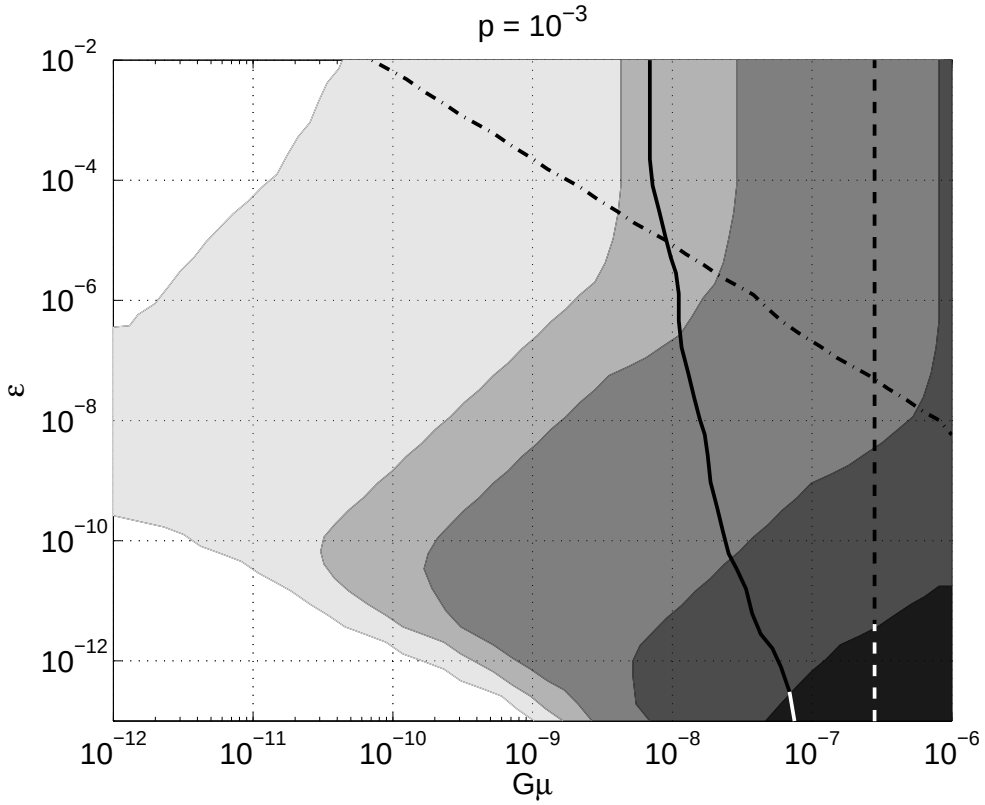

Fig. 15.— The ϵ - $G\mu$ plane for the cosmic string models with $p = 10^{-3}$. The shaded regions are regions excluded by different LIGO results or regions accessible to future LIGO runs. From darkest to lightest, they are: S3 upper limit; S4 upper limit; expected LIGO sensitivity for the H1L1 pair, assuming design interferometer strain sensitivity, and 1 year of exposure; expected LIGO sensitivity for the H1H2 pair, assuming design interferometer strain sensitivity, and 1 year of exposure; expected Advanced LIGO sensitivity for the H1H2 pair, assuming 10× better interferometer strain sensitivity than LIGO design, and 1 year of exposure. The dash-dotted black curve is the exclusion curve based on the pulsar limit (McHugh et al. 1996) (the excluded region is above the curve). The solid black curve is the exclusion curve based on the indirect big-bang-nucleosynthesis bound (the excluded region is to the right of the curve). The vertical black dashed line is the upper limit on $G\mu$ from 3-year WMAP data (Fraisse 2006).

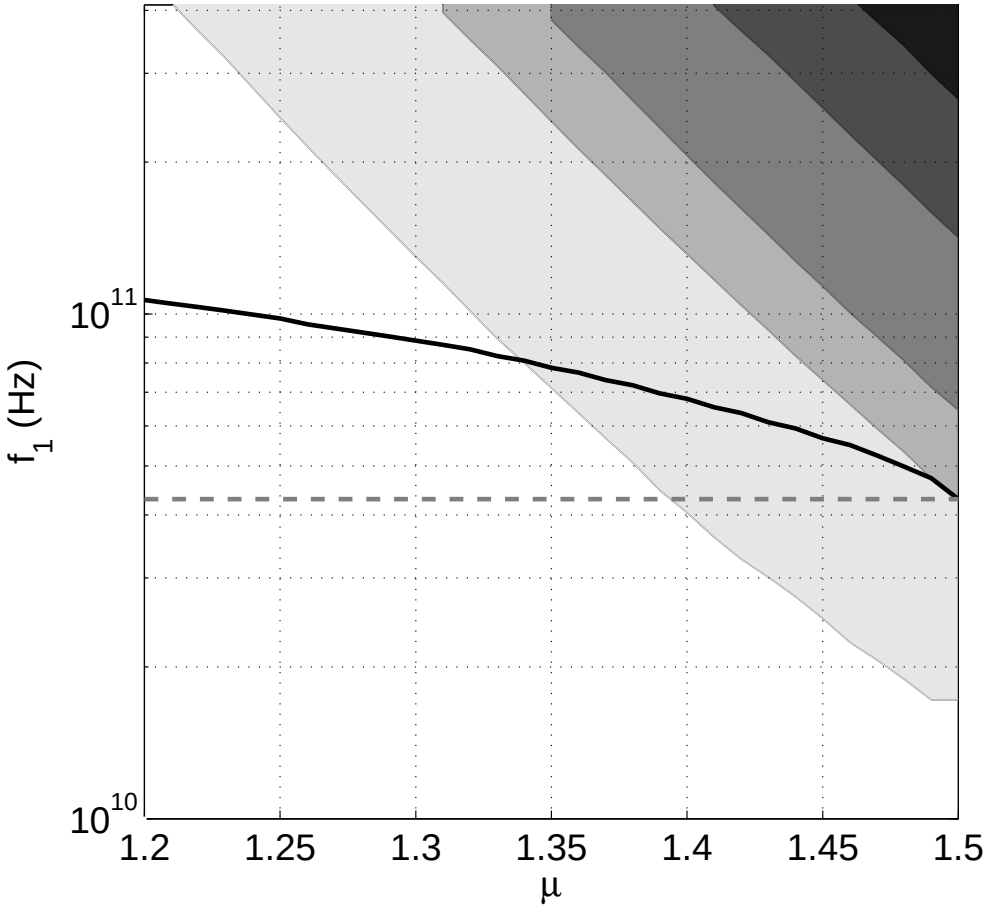

Fig. 16.— The $f_1 - \mu$ plane for the pre-big-bang models with $f_s = 30$ Hz. The shaded regions are regions excluded by different LIGO results or regions accessible to future LIGO runs. From darkest to lightest, they are: S3 upper limit; S4 upper limit; expected LIGO sensitivity for the H1L1 pair, assuming design interferometer strain sensitivity, and 1 year of exposure; expected LIGO sensitivity for the H1H2 pair, assuming design interferometer strain sensitivity, and 1 year of exposure; expected Advanced LIGO sensitivity for the H1H2 pair, assuming 10× better interferometer strain sensitivity than LIGO design, and 1 year of exposure. The black curve is the exclusion curve based on the BBN limit (the excluded region is above the curve). The horizontal dashed line denotes the most natural value of $f_1 = 4.3 \times 10^{10}$ Hz.

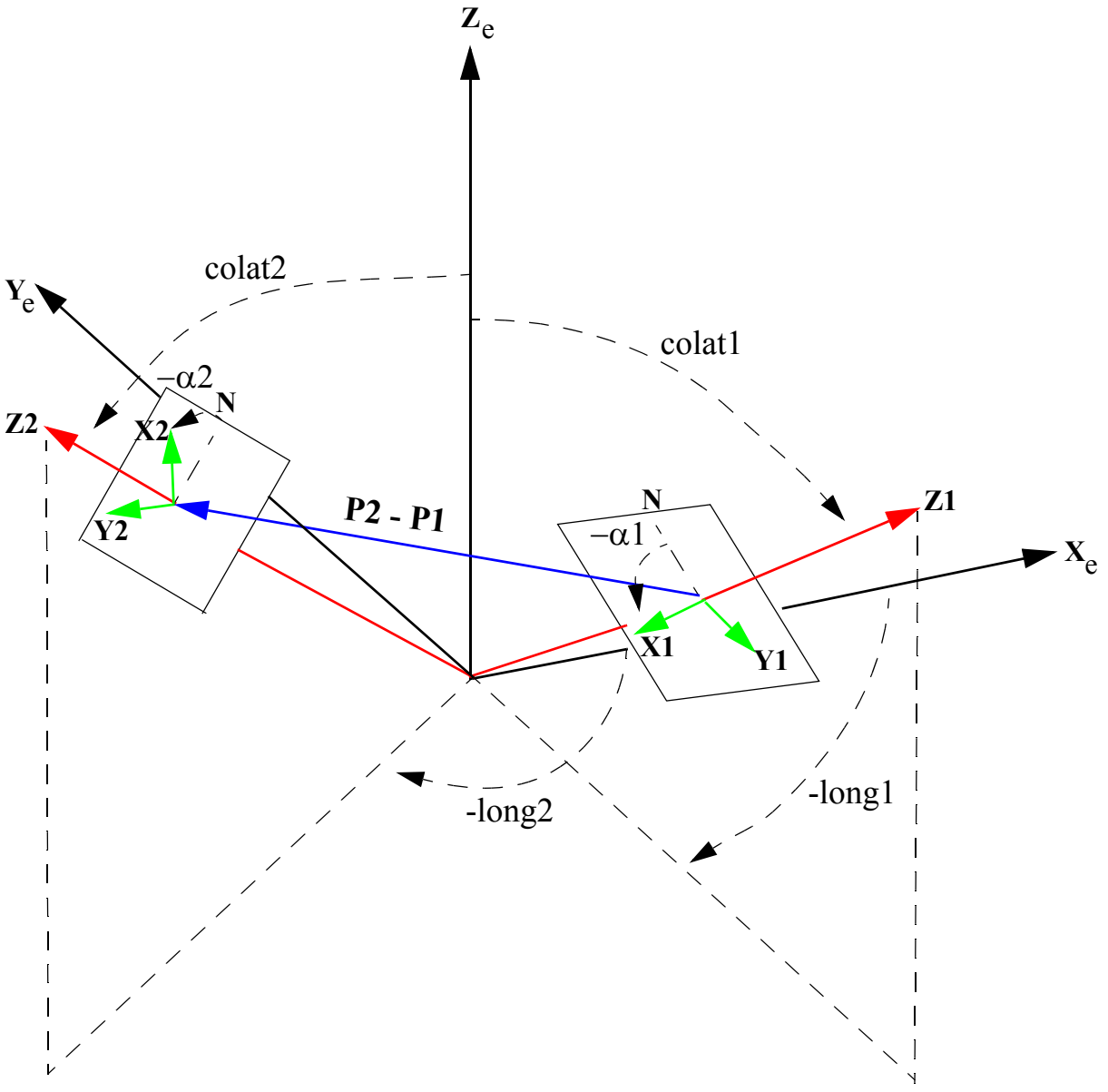
Z_e
Y_e
X_e
colat2
colat1
−α2
N
Z2
X2
Y2
P2 - P1
N
−α1
Z1
X1
Y1
-long2
-long1

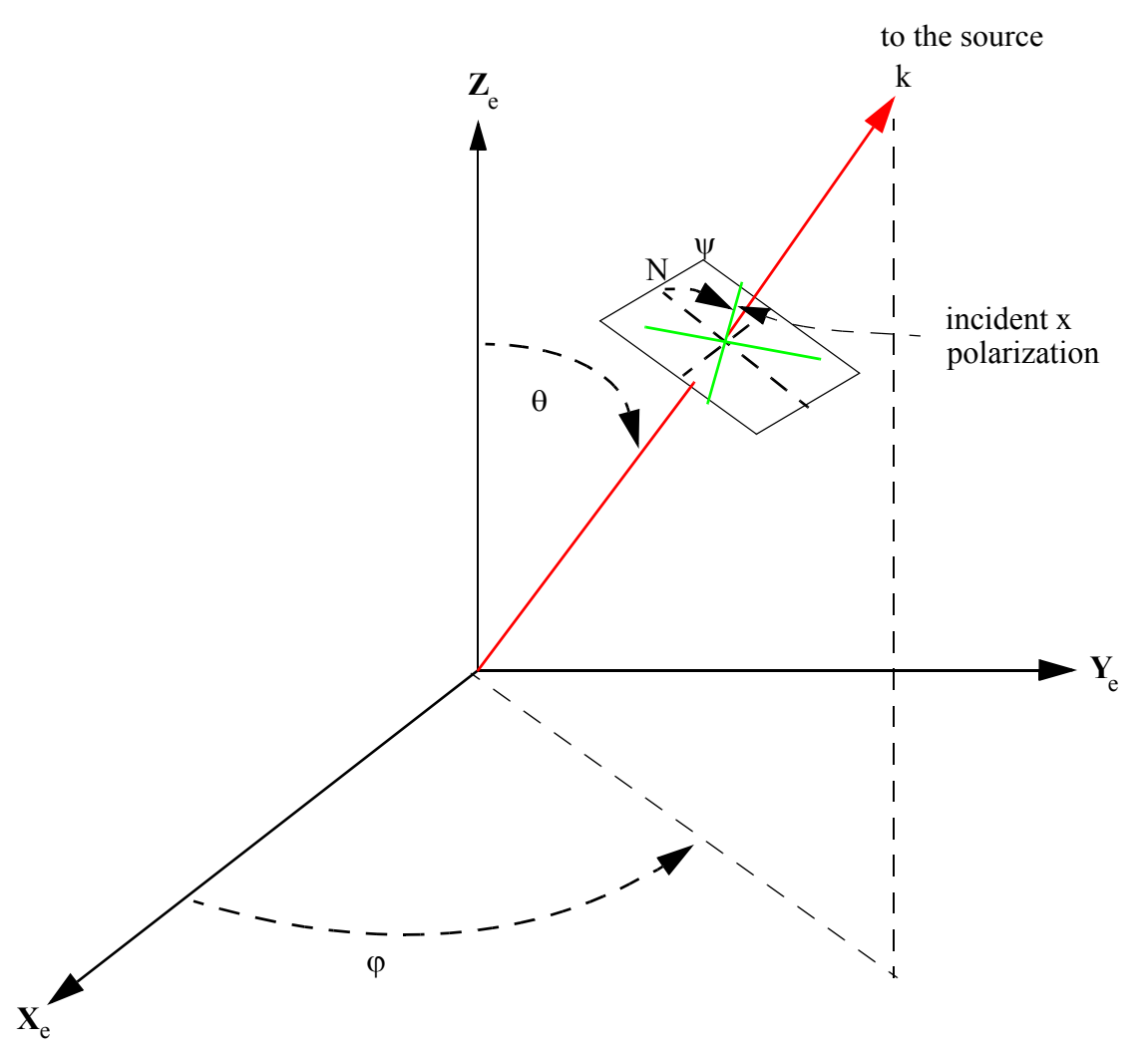
to the source
k
Z_e
ψ
N
incident x
polarization
θ
Y_e
φ
X_e

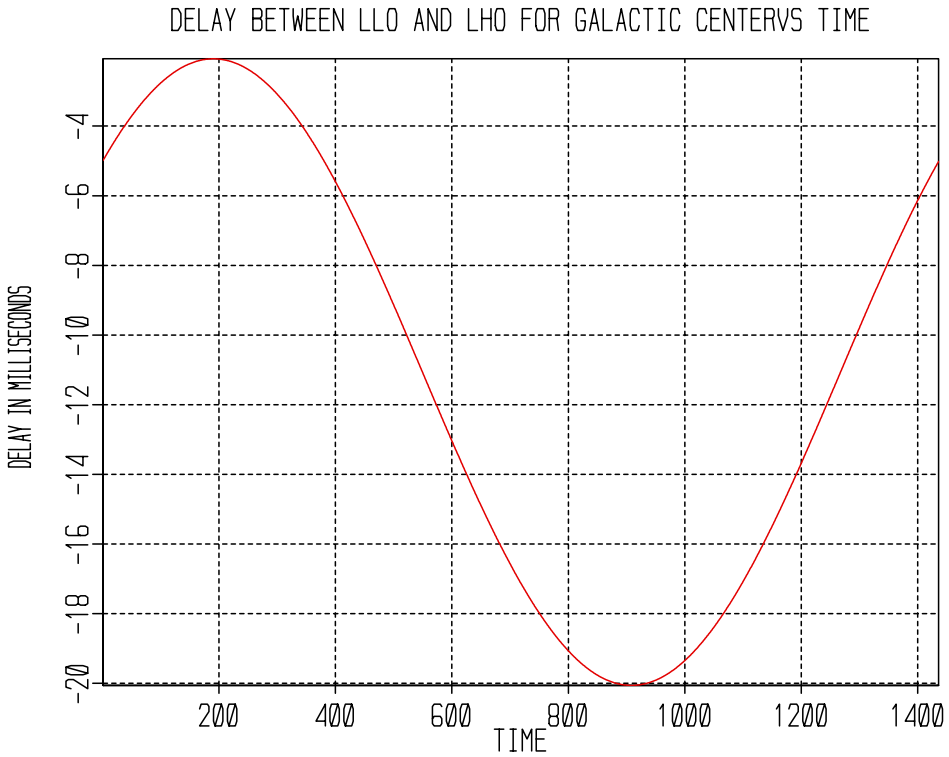

TIME DELAY BETWEEN LLO AND LHO VS MINUTES OF THE SIDEREAL DAY

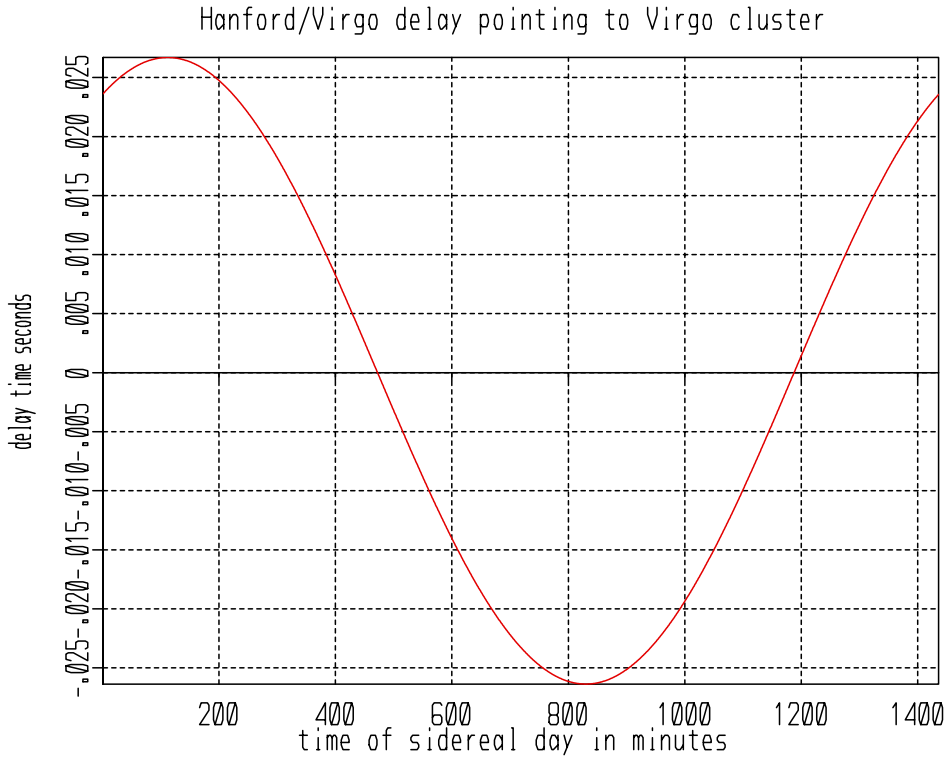

TIME DELAY BETWEEN LHO AND VIRGO VS MINUTES OF THE SIDEREAL DAY

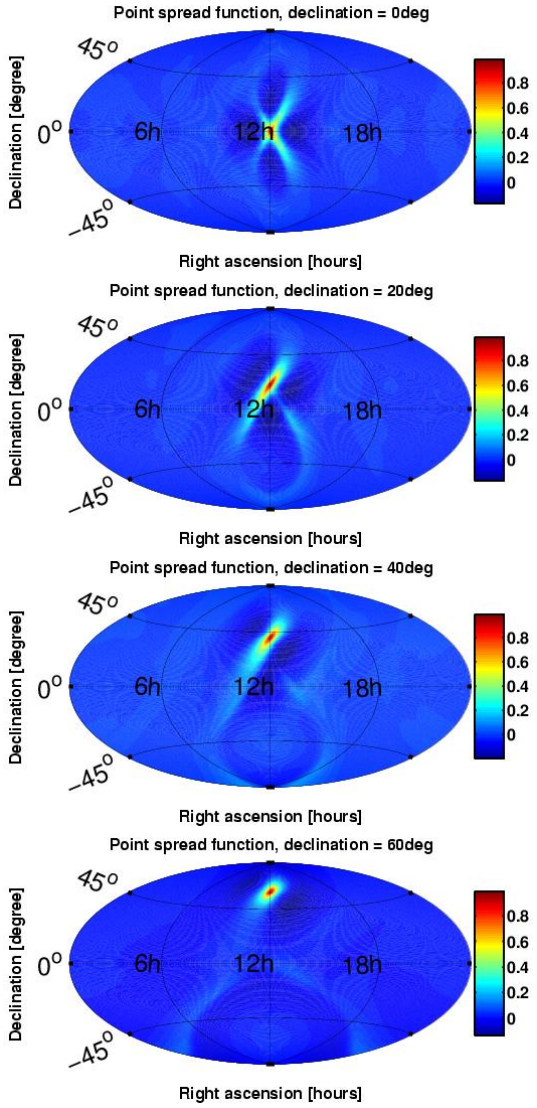

FIG. 2: **Point spread function** $A(\hat{\Omega}, \hat{\Omega}')$ of the radiometer for a flat source spectrum (H = const). Plotted is the expected signal strength assuming a source at right ascension 12 h and declination 0 deg, 20 deg, 40 deg and 60 deg. Uniform day coverage was assumed, so the resulting shapes are independent of right ascension. Typical S4 interferometer power spectra were assumed.

- *Spherical harmonics decomposition* of the SNR map. The resulting power vs l graph shows structure up to roughly $l = 9$ and falls of steeply above that - the $l = 9$ point corresponds to one twentieth of the maximal power. The effective number of independent points then is $N_{\rm eff} \approx (l+1)^2 = 100$.
- *FWHM area* of a strong injected source, which is latitude dependent but of the order of 800 deg^2. To fill the sky we need about $N_{\rm eff} \approx 50$ of those patches. We used the higher estimate $N_{\rm eff} = 100$ for this discussion.

FIG. 3 suggests that the data is consistent with no

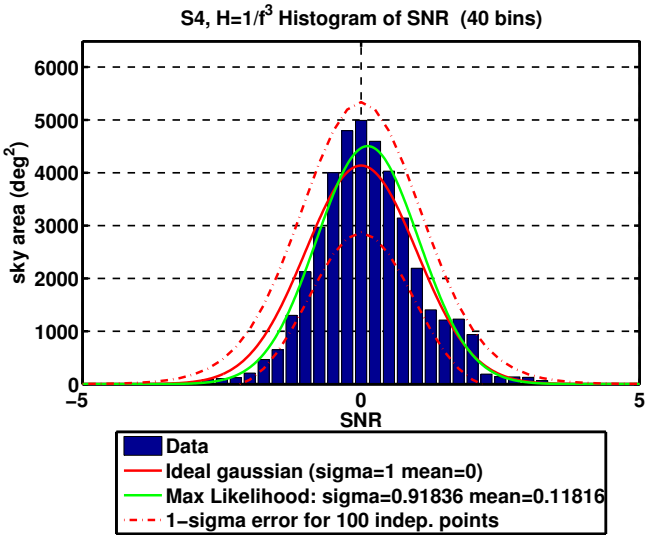

FIG. 3: **S4 Result:** Histogram of the bias corrected signal-to-noise ratio (SNR) for $H(f) = 1\ \mathrm{Hz}^2 f^{-3}$. The green curve is a maximum likelihood Gaussian fit to the data. The red solid line is an ideal Gaussian, the two dash-dotted red lines are the 1-σ bands around the ideal Gaussian for $N_{\rm eff} = 100$.

signal. Thus we calculated a Bayesian 90% upper limit for each sky direction. The prior was assumed to be flat between zero and infinity. Additionally we marginalized over the calibration uncertainty of 8 % for H1 and 5% for L1 using a Gaussian probability distribution. The resulting upper limit map is shown in FIG. 4. The upper limits on the strain power spectrum $H(f)$ vary between $1.2 \times 10^{-48}\mathrm{Hz}^{-1}\,(100\ \mathrm{Hz}/f)^3$ and $1.2 \times 10^{-47}\mathrm{Hz}^{-1}\,(100\ \mathrm{Hz}/f)^3$, depending on the position in the sky.

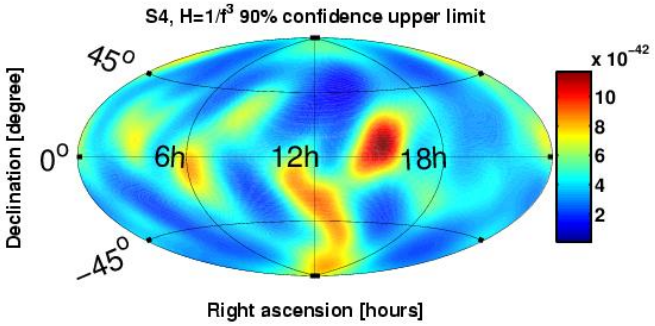

FIG. 4: **S4 Result:** Map of the 90 % confidence level Bayesian upper limit for $H(f) = 1\ \mathrm{Hz}^2 f^{-3}$. The upper limit varies between $1.2 \times 10^{-48}\mathrm{Hz}^{-1}\,(100\ \mathrm{Hz}/f)^3$ and $1.2 \times 10^{-47}\mathrm{Hz}^{-1}\,(100\ \mathrm{Hz}/f)^3$, depending on the position in the sky. All fluctuations are consistent with the expected noise.

2. Constant strain power

Similarly, FIG. 5 shows a histogram of the bias-corrected SNR $= \frac{Y}{\sigma}$ for the constant strain power case. Structure in the spherical harmonics power spectrum goes up to $l = 19$, thus $N_{\rm eff}$ was estimated to be $N_{\rm eff} \approx (l+1)^2 = 400$. Alternatively the FWHM area of a strong injection covers about 100 deg^2 which also leads to $N_{\rm eff} \approx 400$. The dash-dotted red lines in the histogram (FIG. 5) correspond to the expected $1-\sigma$ deviations from the ideal Gaussian for $N_{\rm eff} = 400$. The histogram is thus consistent with (correlated) Gaussian noise, indicating that there is no signal present. The SNR distribution also passes a Kolmogorov-Smirnov test for $N_{\rm eff} = 400$ ($\alpha = 0.1$).

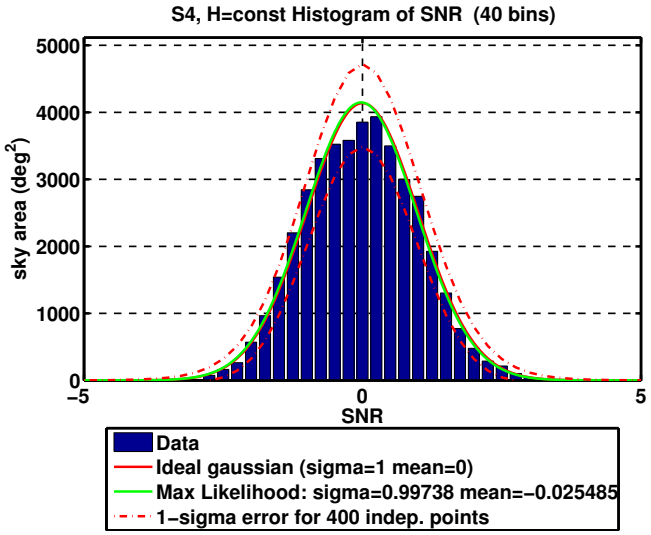

FIG. 5: **S4 Result:** Histogram of the bias corrected signal-to-noise ratio (SNR) for $H(f) = 1$ Hz^{-1}. The green curve is a maximum likelihood Gaussian fit to the data. The red solid line is an ideal Gaussian, the two dash-dotted red lines are the $1-\sigma$ bands around the ideal Gaussian for $N_{\rm eff} = 400$.

Again we calculated a Bayesian 90% upper limit for each sky direction, including the marginalization over the calibration uncertainty. The prior was assumed to be flat between 0 and ∞. The resulting upper limit map is shown in FIG. 6. The upper limits on the strain power spectrum $H(f)$ vary between 8.5×10^{-49}Hz^{-1} and 6.1×10^{-48}Hz^{-1} depending on the position in the sky.

3. Interpretation

The maps presented in FIG. 4 and 6 represent the first directional upper limits on a stochastic gravitational wave background ever obtained. They are consistent with no gravitational wave background being present.

One can interpret this result in terms of potential sources. As an example we look at the gravitational luminosity of all low-mass X-ray binaries (LMXBs) within

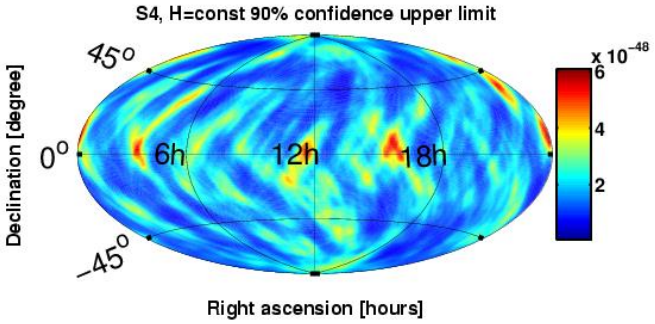

FIG. 6: **S4 Result:** Map of the 90 % confidence level Bayesian upper limit for $H(f) = 1$ Hz^{-1}.The upper limit varies between 8.5×10^{-49}Hz^{-1} and 6.1×10^{-48}Hz^{-1} depending on the position in the sky.

the Virgo galaxy cluster. They have an integrated X-ray luminosity of about 1×10^{-9} erg/sec/cm^2 (3000 galaxies at 15 Mpc, 10^{40} erg/sec/galaxy from LMXBs). For simplicity we assume that they produce a flat strain power spectrum $H(f)$ over a bandwidth Δf. Then the strength of this strain power spectrum is about

$$\begin{aligned} H(f) &= \frac{2G}{\pi c^3} \frac{1}{f_{\rm Kepler} f_{\rm center} \Delta f} F_X \\ &\approx 10^{-55}\ {\rm Hz}^{-1} \left(\frac{100\ {\rm Hz}}{f_{\rm center}}\right)\left(\frac{100\ {\rm Hz}}{\Delta f}\right) \end{aligned} \tag{11}$$

which is out of reach. Here $f_{\rm Kepler} \approx 2$ kHz is final orbital frequency of accreting matter and $f_{\rm center}$ is the typical frequency of the Δf wide band of interest.

B. Limits on isotropic background

It is possible to recover the point estimate and standard deviation for an isotropic background as an integral over the map (see [3]). From that the 90% Bayesian upper limit can be calculated, which is additionally marginalized over the calibration uncertainty. In the $\beta = -3$ case the 90% upper limit we can set on $h^2\Omega_{\rm gw}(f)$ is 6.25×10^{-5}. Table I summarizes the results for all choices of β.

1. Interpretation

The limit on an isotropic stochastic background of gravitational waves that can be set with the S4 data is roughly one order of magnitude lower than the published LIGO S3 limit [1]. In [**?**] LIGO already published an isotropic upper limit using S4 data. While the reconstruction of the isotropic result done here is in principle identical to the analysis presented in [**?**], the actual data cuts were sufficiently different that the result varies slightly. In the future initial LIGO has the

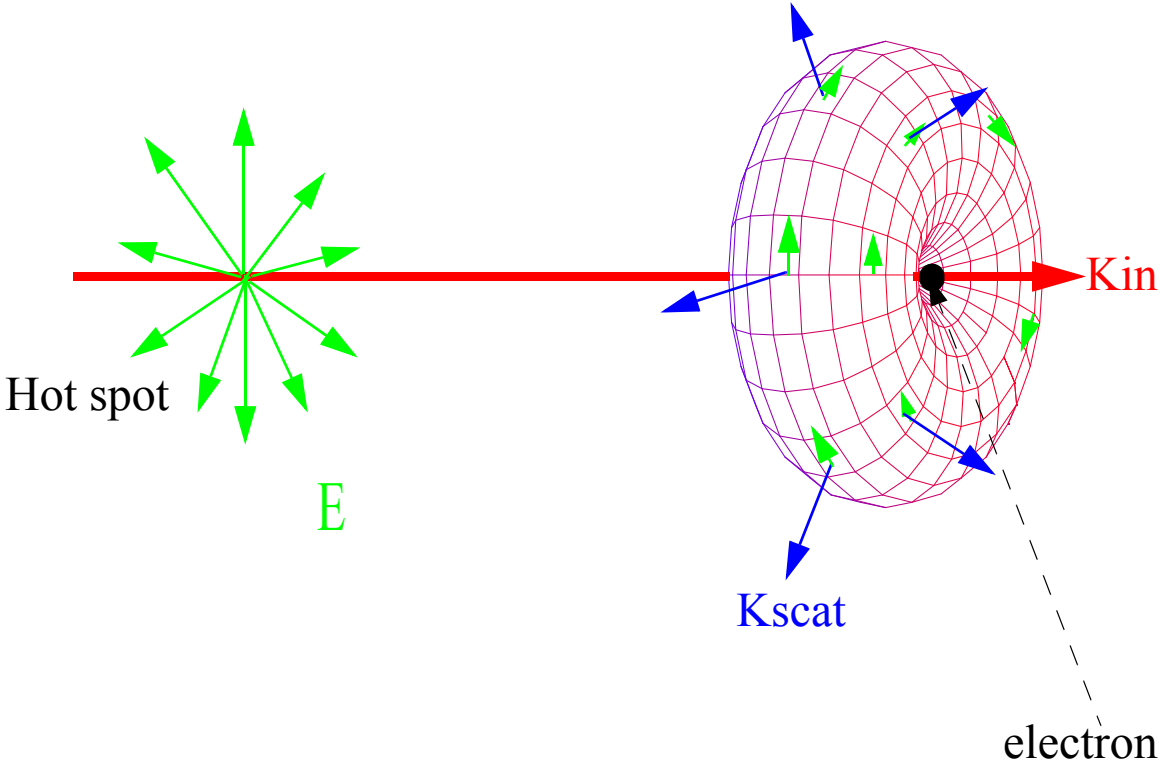
Hot spot
E
Kin
Kscat
electron

H. Edens

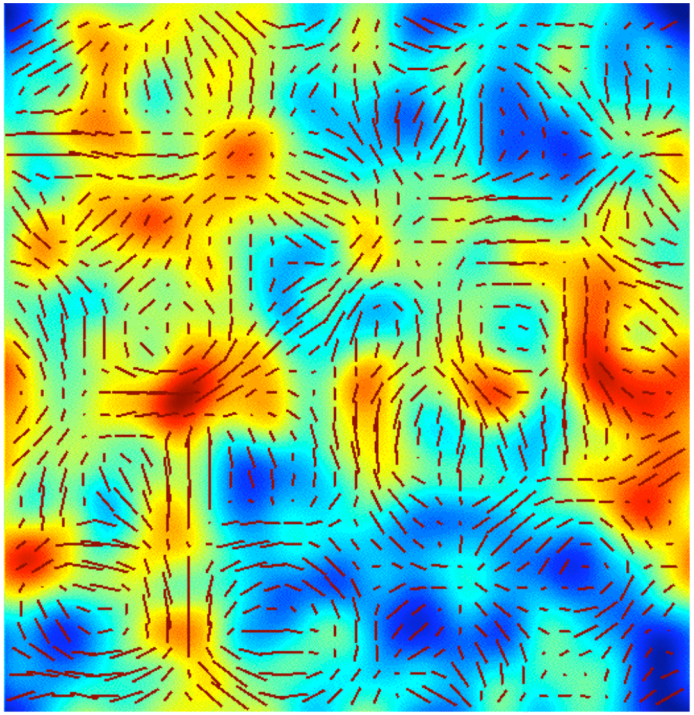

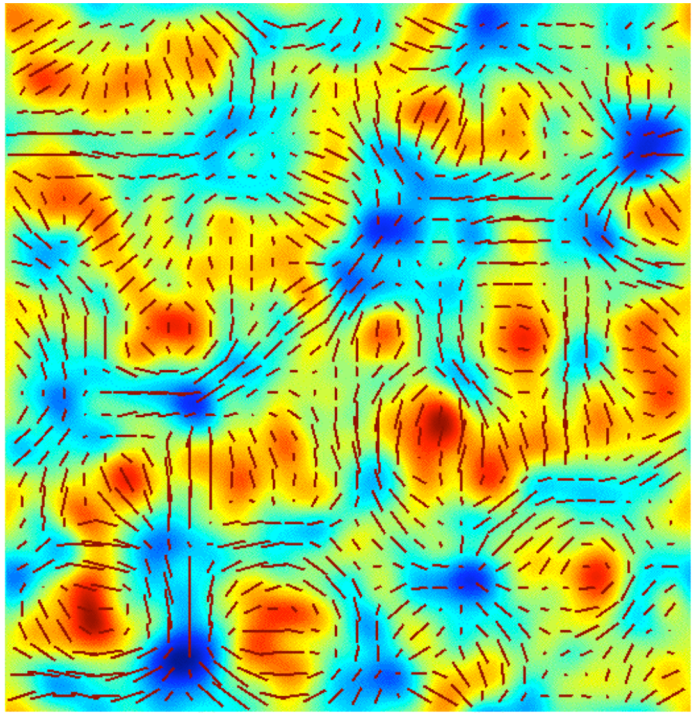

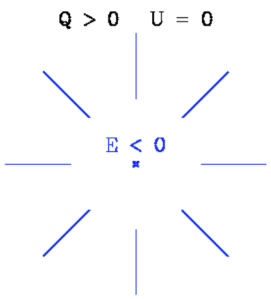

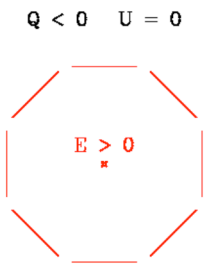

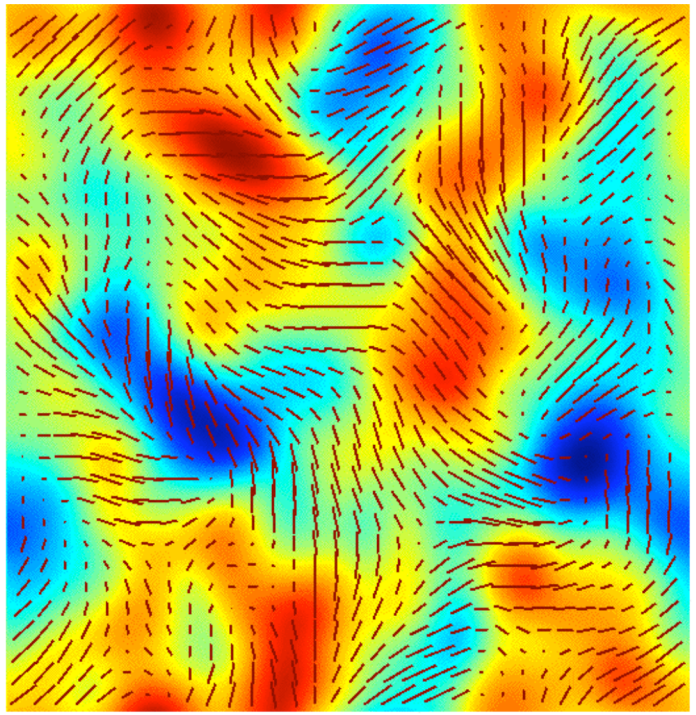

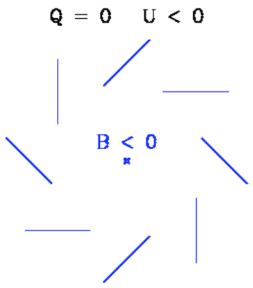

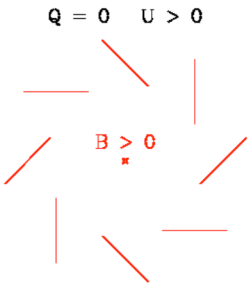

M. Zaldarriaga

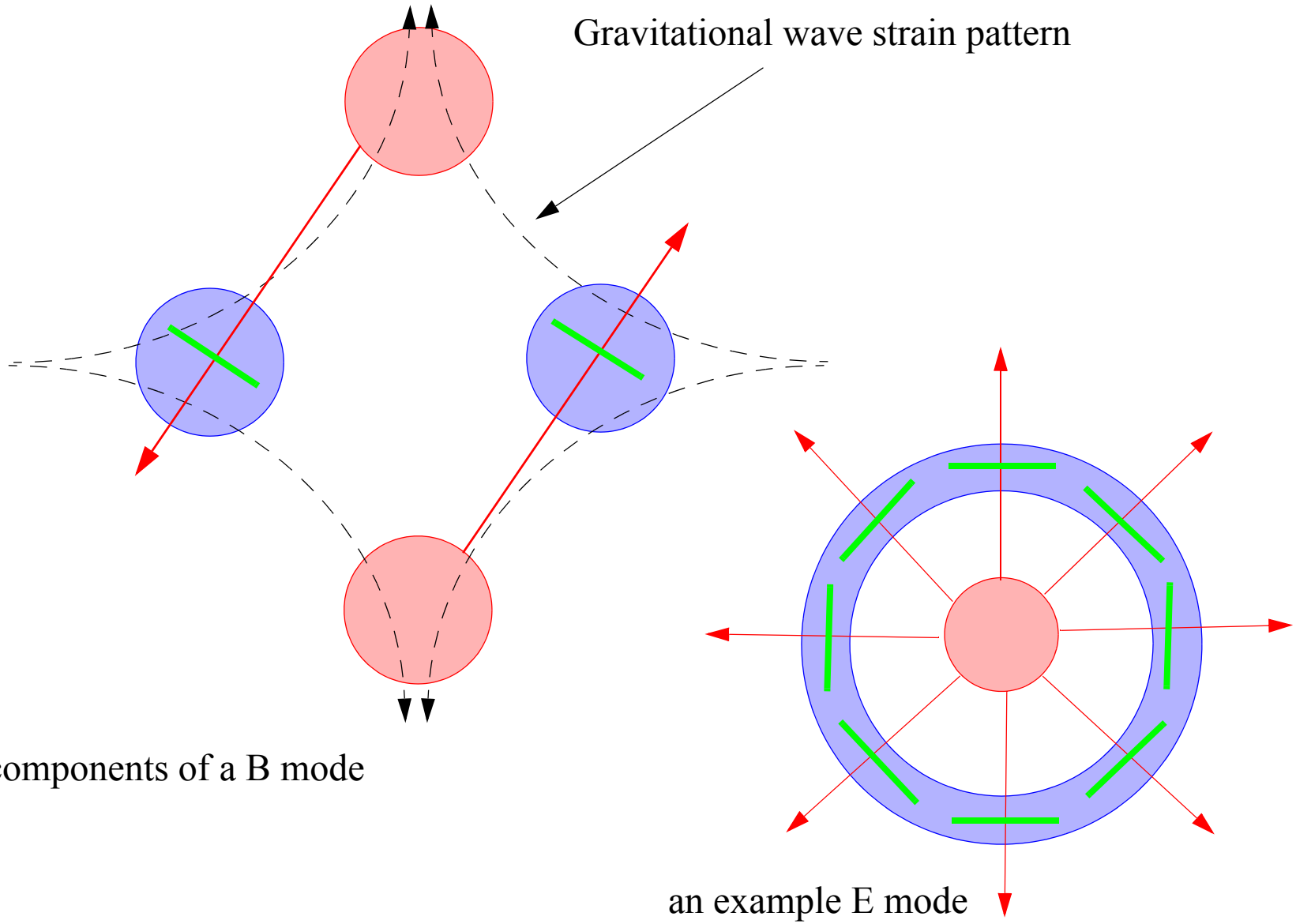
Gravitational wave strain pattern
components of a B mode
an example E mode

Predictions and Limits

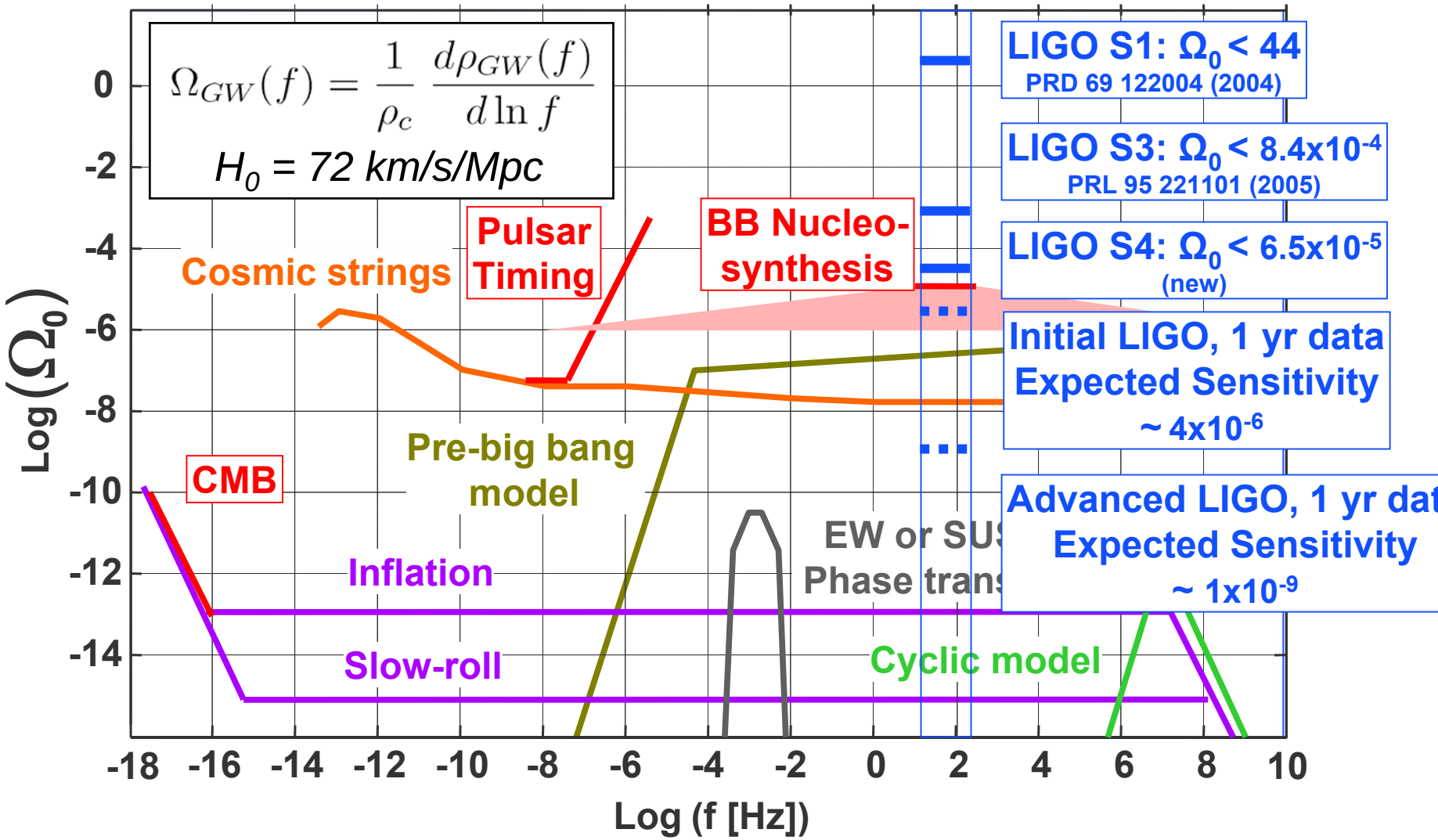

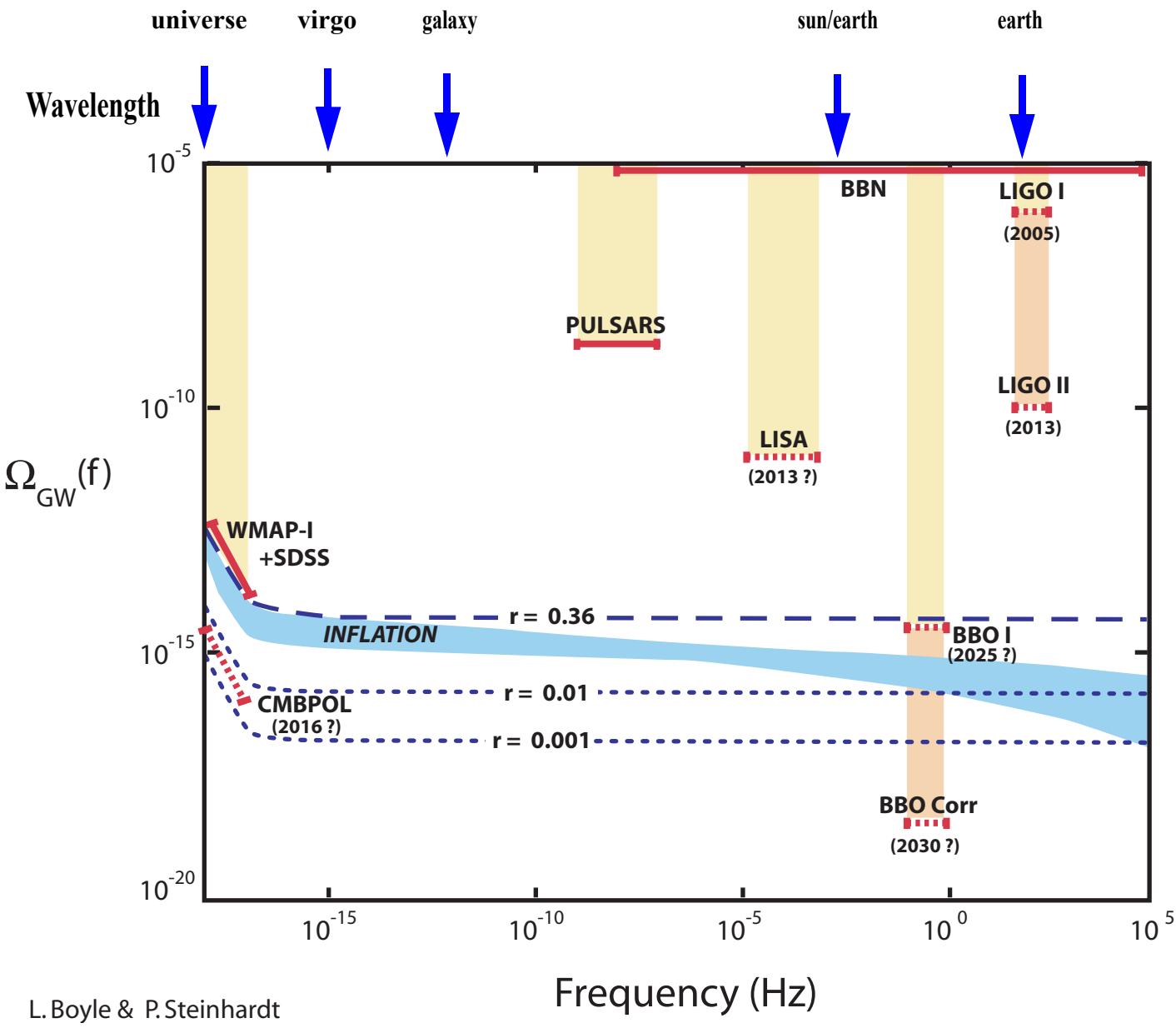

L. Boyle & P. Steinhardt